NeuroImage

www.elsevier.com/locate/ynimg
NeuroImage 23 (2004) 1507–1518

Rapid Communication

Robust unsupervised segmentation of infarct lesion from diffusion tensor MR images using multiscale statistical classification and partial volume voxel reclassification

Wu Li,[a] Jie Tian,[a,*] Enzhong Li,[a] and Jianping Dai[b]

[a]*Institute of Automation, Chinese Academy of Sciences, Beijing 100080, China*
[b]*Department of Neuroradiology, Beijing Tiantan Hospital, Beijing 100050, China*

Received 14 May 2004; revised 31 July 2004; accepted 9 August 2004

Manual region tracing method for segmentation of infarction lesions in images from diffusion tensor magnetic resonance imaging (DT-MRI) is usually used in clinical works, but it is time consuming. A new unsupervised method has been developed, which is a multistage procedure, involving image preprocessing, calculation of tensor field and measurement of diffusion anisotropy, segmentation of infarction volume based on adaptive multiscale statistical classification (MSSC), and partial volume voxel reclassification (PVVR). The method accounts for random noise, intensity overlapping, partial volume effect (PVE), and intensity shading artifacts, which always appear in DT-MR images. The proposed method was applied to 20 patients with clinically diagnosed brain infarction by DT-MRI scans. The accuracy and reproducibility in terms of identifying the infarction lesion have been confirmed by clinical experts. This automatic segmentation method is promising not only in detecting the location and the size of infarction lesion in stroke patient but also in quantitatively analyzing diffusion anisotropy of lesion to guide clinical diagnoses and therapy.

Keywords: Segmentation; DT-MRI; Infarction; Diffusion anisotropy; Statistical classification

Introduction

Stroke is a life-threatening disease associated with long-term disability. It is very important to employ the techniques of diffusion magnetic resonance (MR) imaging, including diffusion weighted magnetic resonance imaging (DW-MRI) and diffusion tensor magnetic resonance imaging (DT-MRI) in stroke diagnosis, especially at the super-acute stage of stroke. To accurately detect the location and size of infarct lesions in stroke patients helps classifying the subtype of stroke (Gonzalez et al., 1999; Lovblad et al., 1998), quantitatively determining the changes in water diffusion anisotropy (Mukherjee et al., 2000; Sorensen et al., 1999; Sotak, 2002), and predicting the clinical condition and eventual outcome (Lovblad et al., 1997; O'Sullivan et al., 2004). Manual region tracing methods are used in previous studies to calculate infarct volume (Baird et al., 1997; Barber et al., 1998; Mukherjee et al., 2000; Sorensen et al., 1999), but manual segmentation of infarct lesion is labor intensive and results are operator dependent.

Automatic or semiautomatic segmentation of infarction lesions in DW-MR or DT-MR images is still a difficult issue because of noise, intensity overlapping, partial volume effect (PVE), and intensity shading artifacts. The existing PVE is due to limited spatial resolution of the scanner. Intensity shading artifacts are caused by radio frequency (RF) inhomogeneities. Intensity overlapping is caused by similar intensity of infarct lesion and nerve tracts, which is still an unsolved problem.

The literature about automatic or semiautomatic segmentation of brain infarct lesion is quite limited. Martel et al. (1999) used a semiautomatic method to determine infarct volume by DW-MRI. An adaptive threshold algorithm incorporating a spatial constraint was used to segment the images. But the misclassification between susceptible artifacts and nerve tracts cannot be well distinguished. In fact, the misclassification of nerve tract results from intensity overlapping in DW-MRI images.

To resolve the problem of segmentation of pathological region in conventional MR images, atlas-based segmentation technique has been used (Leemput et al., 1999a, 2001; Moon et al., 2002; Warfield et al., 1999, 2000). Anatomical templates have been successfully employed to identify anatomical structures through nonlinear registration. Leemput et al. (1999b) developed an automatic segmentation method for magnetic resonance (MR) image of normal brains by statistical classification using an atlas as prior knowledge for initialization and also for geometric con-

---

* Corresponding author. Medical Imaging Processing Group, Institute of Automation, Chinese Academy of Sciences. No. 95 Zhongguancun East Road, Beijing 100080, China. Fax: +86 10 62527995.

E-mail address: tian@doctor.com (J. Tian).

1053-8119/$ - see front matter © 2004 Elsevier Inc. All rights reserved.
doi:10.1016/j.neuroimage.2004.08.009

straints. Recent extension, detecting brain lesions as outliers (Leemput et al., 2001), was successfully applied in detection of multiple sclerosis lesions. Based on the work of Leemput et al., Moon et al. (2002) modified spatial atlas to include prior probabilities for pathology region. Although atlas-based segmentation methods look good in pathological region segmentation from conventional MR images, it is hard to segment the infarct region from diffusion MR images due to overlapping intensities between infarction lesion and normal tissue.

Some approaches have been applied to address the problem of partial volume (PV) segmentation. Laidlaw et al. (1998) used histograms taken over voxel-sized regions to represent the contents of the voxels and identified the mixture of material within the voxel using a probabilistic Bayesian approach. The Bayesian approach matches the histogram by finding the mixture of materials within each voxel, which is most likely to have created the histogram. But it is not clear how many tissues a voxel contains for PV distribution, and RF inhomogeneities are assumed to be negligible. Shattuch et al. (2001) and Noe and Gee (2001) marginalized over the variables describing the fractional portions of each pure tissue class and dealt with PV voxels as new set of PV classes. An additional estimation step is necessary to obtain the fractional amount of pure tissues in each voxel; and the method may also oversmooth the classification result.

In this paper, we present a new adaptive unsupervised method to segment brain infarct lesion from one of the original DT-MR images of stroke patients, acquired at more than six directions, based on Bayesian probability theory and partial volume voxel reclassification (PVVR). The method accounts for random noise, intensity overlapping, PVE, and intensity shading artifacts. The method is a multistage process, involving first images preprocessing, second calculation of diffusion tensor and diffusion anisotropy from DT-MR images, third segmentation of infarction volume based on region splitting and merging and adaptive multiscale statistical classification (MSSC), and finally partial volume voxel reclassification (PVVR). The proposed adaptive MSSC model accounts for spatial, intensity gradient, diffusion anisotropy, and contextual information of original DT-MR images of the patient. The proposed PVVR model makes segmentation more accurate by using local parameter information.

Materials and methods

Diffusion MR imaging

DT-MRI is a technique for measuring the anisotropic diffusion properties of water molecules in biological tissues. Twenty patients with clinically diagnosed brain infarction by DT-MRI scanning were used in this study. The scans were obtained by 1.5 or 3.0 T MRI scanner (GE Medical System, Milwaukee, USA; Siemens, Erlangen, Germany) using diffusion tensor echo planar imaging with 13 different motion probing gradient directions (TR/TE: 6000–7000/98 ms, matrix: 128 × 128, FOV: 24 cm, slice thickness 5 mm, b value: 1000 s/mm^2). The image used for segmentation is 1 of the 13 original DT-MR images acquired.

Image preprocessing

Before calculating the diffusion tensors from DT-MR images, the images were restored by using a nonlinear anisotropic diffusion filter (Perona and Malik, 1990) that reduces white noise while preserving edges and partial volume effects.

Estimation of diffusion tensor and diffusion anisotropy from DT-MR images

Diffusion is a three-dimensional process and the molecular mobility may not be the same in all directions (Le Bihan and Mangin, 2001; Westin et al., 2002; Wiegell, 2003). The proper way to study anisotropic diffusion is to consider the diffusion tensor. Diffusion is no longer characterized by a single scalar coefficient but a tensor D, which fully describes molecular mobility along each axis and the correlation between these axes:

$$D = \begin{bmatrix} D_{xx} & D_{xy} & D_{xz} \\ D_{yx} & D_{yy} & D_{xx} \\ D_{zx} & D_{zy} & D_{zz} \end{bmatrix}$$

The calculation of tensor D is complex and described in detail by Le Bihan and Mangin (2001). Fig. 1 presents a "slice" of the diffusion tensor volume data from an acute stroke patient. Each subimage indicates the scalar values of the associated diffusion tensor component.

Traditional approaches to diffusion tensor imaging involve converting the tensors into eigenvalue/eigenvector representation that is rotationally invariant. Every tensor may then be interpreted as an ellipsoid with principal axes oriented along the eigenvectors and radii equal to the corresponding eigenvalues. The ellipsoid describes the probabilistic distribution of a water molecule after a fixed diffusion time.

Using eigenvalues/eigenvectors, one can compute different anisotropy measures (Le Bihan and Mangin, 2001; Westin et al., 2002) to map tensor data onto scalars and to quantitatively estimate the diffusion anisotropy. The most commonly used invariant indices are the fractional anisotropy (FA).

$$\mathrm{FA} = \sqrt{3\left[(\lambda_1 - \mathrm{Tr}(D))^2 + (\lambda_2 - \mathrm{Tr}(D))^2 + (\lambda_3 - \mathrm{Tr(D)})^2\right]} \Big/ \sqrt{2\left(\lambda_1^2 + \lambda_2^2 + \lambda_3^2\right)} \tag{1}$$

$$\mathrm{Tr}(D) = (\lambda_1 + \lambda_2 + \lambda_3)/3 \tag{2}$$

where Tr(D) is the trace of the diffusion tensor D, which represents the mean diffusivity. Fig. 2 illustrates the measures of the trace Tr(D) and diffusion anisotropy FA. From Fig. 2b, we can see that the diffusion anisotropy is higher in white matter (WM) than in gray matter (GM) or in cerebrospinal fluid (CSF).

Scale space

In recent years, multiscale approaches in image analysis have been proven as an effective method in terms of describing images at varying levels of resolution (Escoda et al., 2002; Schnabel and Arridge, 1996). The underlying image can be represented by a family of images at different levels of inner spatial scale. Global structure properties are extracted from the image and smaller scale features are suppressed at large scales. The detailed structure characteristics become more prominent at lower scales. Scale space of original DT-MR image at one direction will be constructed.

Fig. 3 illustrates scale-space stack (Escoda et al., 2002). It is composed of successive versions of the original DT-MR data set at

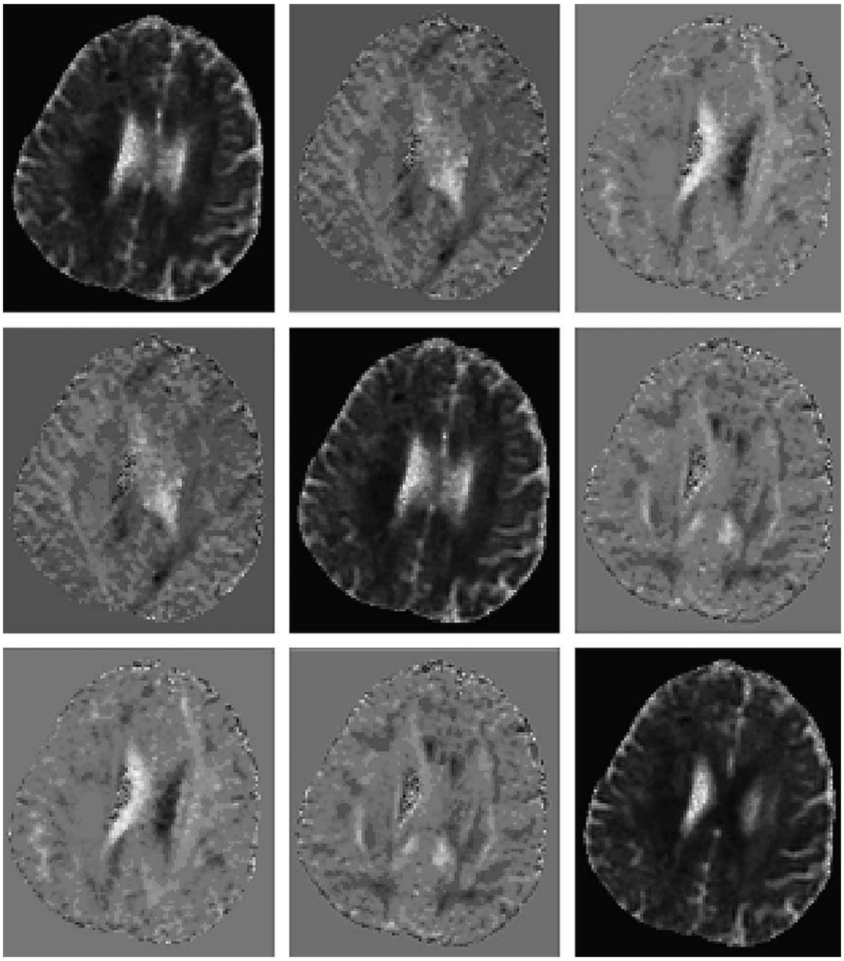

Fig. 1. Slice of a diffusion tensor volume. Every element of the image corresponds to one component of the tensor. The tensor field was calculated from original DT-MR images with 13 directions of an acute stroke patient.

coarser scales. It is assumed that the bigger the scale is, the less information referred to local characteristics of the input data will appear. General information applying to large scales will last through scale (Escoda et al., 2002). Different scale level t represents different image spatial resolution. Scale level $t = 0$ indicates the original DT-MR image. With increasing scale level, the image is more blurring and contains less information. It is reasonable to believe that local and high-resolution scale information may be related to general and low-resolution scale information. This will enable us to extract image structure.

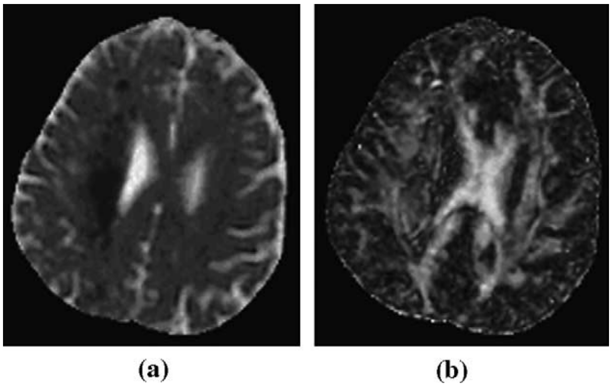

Fig. 2. Measurements of the trace Tr(D) and diffusion anisotropy FA. (a) The trace map. (b) FA map.

Scale space can be generated by different principles. Linear scale-space technique blurs important image features such as edges. Nonlinear scale space overcomes this major drawback and encourages intraregion smoothing in preference to inter-region smoothing. Perona and Malik (1990) proposed a partial differential equation model. The main idea is to introduce a part of edge detection step in the filtering itself, allowing an interaction between scales from the beginning in the algorithm. They replaced the heat

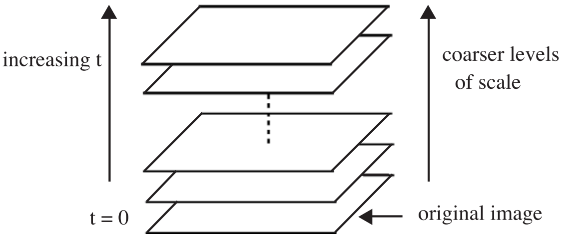

Fig. 3. Illustration of scale-space stack (Escoda et al., 2002). Scale space is composed by the stack of successive versions of the original data set at coarser scales. The bigger the scale level, the less information referred to local characteristics of the input data will appear. Scale level $t = 0$ indicates the original image.

equation by a nonlinear equation. The anisotropic diffusion equation is

$$\frac{\partial}{\partial t}y(i,t) = \mathrm{div}(c(i,t)\nabla y(i,t)) = c(i,t)\Delta y(i,t) + \nabla c \cdot \nabla y(i,t) \quad (3)$$

In our case, $y(i,t)$ stands for the blurred intensity of original DT-MR image on position i and at scale level t; $c(i, t)$ is the diffusion coefficient, which is assumed to be a variant dependent of the space location.; we indicate div as the divergence operator, and ∇ and Δ are, respectively, as the gradient and Laplacian operators with respect to the space variables.

The diffusion coefficient is chosen locally as a function of the magnitude of the gradient of the brightness function.

$$c(i,t) = g(|\nabla y(i,t)|) \quad (4)$$

Different functions were used for $g(\cdot)$ giving perceptually similar results. The following diffusion function is used in our algorithm to generate scale space

$$g(|\nabla y(i,t)|) = e^{\left(-\left(|\nabla y(i,t)_l|/\mathrm{Ks}\right)^2\right)} \quad (5)$$

The constant Ks is fixed either by hand at some fixed value or using the "noise estimator" described by Canny (1986).

Scale space of original DT-MR data set is generated before segmentation, and the number of scale level n is confirmed by experience. Using anisotropic diffusion filter, a series of images with different and consecutive definition were obtained for generating the scale space. With increasing scale level, image is more blurred. For the original DT-MR image with no blurring, scale level t equals 0 ($t = 0$). The series images in scale space will not be subsampled as the scale changes. The segmentation result at higher scale level $t + 1$ will be used to initialize the segmentation at scale level t; when we get the segmentation at scale level 0 ($t = 0$), the optimal segmentation result is obtained. Here DT-MR image at scale level t is denoted by $y(t) = (y(i,t), i \in I)$, and the corresponding segmentation is then denoted by $x(t) = (x(i,t), i \in I)$.

Multiscale statistical classification (MSSC)

For original DT-MR images of acute or subacute stroke patient, infarction lesion shows high intensity; and WM and GM have similar gray intensity. Our purpose is to detect the location and the size of infarction lesion so we will divide the original image into three classes, background and CSF, WM and GM, and infarction lesion.

Using anisotropic diffusion filter, a series of images with different resolution was obtained. The nonlinear anisotropic diffusion effectively counters RF inhomogeneities by smoothing the brain regions. The detail decreases with the increased scale level. The set of coordinates of the voxel sites in the image is denoted by I. The blurred image series is represented by $y(t)$, $t \in N$, $N = \{1,2,\ldots,n\}$ (t is the number of scale level, and n is the maximum of t); $y_i(t)$ denotes the image intensity at the voxel site indexed by i at scale level t. Segmentation of the image is an assignment of the correct tissue class in every voxel. The total number of tissue classes in the image is K and each tissue class is represented by a label from $\Lambda = \{1,2,\ldots,k\}$. If $x_i(t)$ denotes an instance of random variable that represents the tissue class at the voxel site i, $x_i(t) = k$ indicates that the tissue class k is assigned to the voxel site i at scale level t. A segmentation on $y(t)$ is then denoted by x at scale level $t = (x_i(t), i \in I)$. The process of segmentation is to find $x(0)$ that represents the correct tissue class at each voxel site given by original image $y(0)$.

To obtain the optimal segmentation $x(t)$ of $y(t)$, we attempt to model $p(y(t) \mid x(t))$ (the measurement model) and $p(x(t))$ (the prior model), which is similar to the method of maximum a posterior (MAP) estimation (as described in Appendix). We assume that the noise is additive, white, Gaussian, tissue dependent, and space variant (Rajapakse et al., 1997). With the assumption, we can get the measurement model $p(y(t)|x(t))$. The measurement model is characterized by the parameter set $\theta(t) = \{\theta_i(t), i \in I\}$ $t \in N$, $N = \{1,2,\ldots,n\}$, where $\theta_i(t) = \{\theta_{k,i}(t) = (\mu_{k,i}(t), \sigma_{k,i}(t)), k \in \Lambda\}$, and $\mu_{k,i}(t)$, $n_{k,i}(t)$, and $\sigma_{k,i}(t)$ that represent the mean image intensity of class k at site i, the noise signal at site i for tissue class k, and the standard deviation of the noise for the tissue class k at site i at scale level t, respectively.

If the segmentation $x(t + 1)$ is obtained at scale level $t + 1$, the parameters $\theta(t + 1)$ can be estimated accordingly. With the known parameters $\theta(t + 1)$ used at scale level t, we get new segmentation of image $y(t)$ at scale level t. The parameters $\theta(t + 1)$ of segmentation $x(t + 1)$ at scale level $t + 1$ is used to get the next segmentation at t. After n iterations of segmentation and parameter estimation, when we reach the original image ($t = 0$) with the finest spatial resolution of the image series, the final optimal segmentation is acquired. Therefore, segmentation can be expressed in two-step process:

$$\hat{x}(t) = \arg\min_{x(t)} U\left(x(t)|y(t), \hat{\theta}(t+1), \hat{x}(t+1)\right) \quad (6)$$

$$\hat{\theta}(t) = \arg\max_{\theta(t)} p(y(t)|\hat{x}(t), \theta(t+1)) \quad (7)$$

where the hat indicates an estimation. In Eq. (6), we estimate the most likely segmentation given the model parameters for each class; and in Eq. (7), we estimate the model parameters given the segmentation. The measurement model parameters are chosen to maximize the likelihood of the image data. MSSC procedure converges to a minimum of energy function $U(x)$, after tissue classes are determined over the image for all iterations. Similar to the definition of energy function by Rajapakse et al as described by Eq. (23) in Appendix, we get energy function $U(x(t))$ at scale level t.

$$\begin{aligned} U(x(t)) = {} & \frac{1}{2}\sum_k \sum_{i \in R_k} \left(\frac{y_i(t) - \mu_{k,i}(t+1)}{\sigma_{k,i}(t+1)}\right)^2 \\ & + \sum_k \sum_{i \in R_k} \log\left(\sigma_{k,i}(t+1)\right) + \beta \sum_{c \in C} \sum_{i \in R_k} V_c(x_i(t+1)) \end{aligned} \quad (8)$$

where R_k represents the voxels that belong to class k. Here, $V_c(x_i(t))$ is the number of voxels where $x_j(t) = x_i(t)$ for i and j are in the clique C. Convergence is decided when the number of changes of the tissue classes at the voxel sites drops below a certain threshold.

In DW-MR or DT-MR images, infarction lesion shows up with high signal intensity while the intensity of nerve tracts is also high. The overlapping intensities make it hard to identify nerve tracts from infarction lesion; therefore, it is hard to accurately detect the infarction volume in stroke patients. We resolve the problem by incorporating diffusion anisotropy into the energy function $U(x(t))$.

$$\alpha_i(t) = |\mu_{k,i}(t) - r_i(t)| \tag{9}$$

$$r_i(t) = a \cdot FA_i(t) \tag{10}$$

$r_i(t)$ represents the effect of diffusion anisotropy $FA_i(t)$ on the original DT-MR image at site i of scale level t. Factor a ensures the same intensity scope of FA as y, which equals to the highest gray value of nerve tract tissue in original DT-MR image data set. $\alpha_i(t)$ is the absolute value of the difference between $y_i(t)$ and $r_i(t)$. At one voxel site i, if $r_i(t)$ is close to the mean gray value of class "infarction lesion", $\alpha_i(t)$ will be little. So $1/\alpha_i(t)$ will be high. To overcome the misclassification of nerve tracts as infarction lesion, here the energy function $U(x(t))$ is changed as follows.

$$U(x(t)) = \frac{1}{2}\sum_k \sum_{i\in R_k}\left(\frac{y_i(t)-\mu_{k,i}(t+1)}{\sigma_{k,i}(t+1)}\right)^2 + \sum_k \sum_{i\in R_k}\log\left(\sigma_{k,i}(t+1)\right) + \beta\sum_{c\in C}\sum_{i\in R_k} V_c(x_i(t+1)) + \sum_k \sum_{i\in R_k}\gamma\cdot\frac{1}{\alpha_i(t)} \tag{11}$$

where γ is a normalizing constant. With the added last term in energy function $U(x(t))$ of Eq. (11), normal nerve tracts can be distinguished from infarction lesion. If one voxel i, which belongs to normal nerve tracts, is misclassified as infarction lesion, the last term in $U_i(x(t))$ will be very high. The bigger γ is used, the more effect is caused by the last term. Voxels are classified by minimizing energy function $U(x(t))$, then the misclassification of nerve tract as infarction lesion can be avoided. Moreover, if this voxel is not classified as infarction lesion but classified as any of the other two classes, the last term in $U(x(t))$ will almost not affect the general energy. Constant coefficient γ is used to adjust the effect of $1/\alpha_i(t)$, which is confirmed by experience. We classify every voxel at scale level t by the minimization of $U(x(t))$, so the misclassification caused by diffusion anisotropy in diffusion image can be avoided.

After the segmentation at scale level t is estimated by minimizing the energy function $U(x(t))$, the measurement model parameters can be calculated accordingly. We can get the measurement model parameter set $\theta(t) = \{\theta_i(t), i\in I\}$ at scale level t, where $\theta_i(t) = \{\theta_{k,i}(t) = (\mu_{k,i}(t), \sigma_{k,i}(t)), k\in\Lambda\}$, by differentiating log $p(y(t)\,|\,x(t), \theta(t+1))$ with respect to $\mu_{k,i}(t)$ or $\sigma_{k,i}(t)$, and equating it to zero. The estimation $\mu_{k,i}(t)$ and $\sigma_{k,i}(t)$ is given by:

$$\mu_{k,i}(t) = \mu_k(t) = \frac{\sum_{i\in R_k} y_i(t)}{|R_k(t)|}, \sigma^2_{k,i}(t) = \sigma^2_k(t) = \frac{\sum_{i\in R_k}\left(y_i(t)-\mu_{k,i}(t)\right)^2}{|R_k(t)|} \tag{12}$$

where $R_k(t)$ denotes the region or the set of all voxel sites belonging to tissue class k at scale level t.

Partial volume voxel reclassification (PVVR)

Shattuch et al. (2001) and Noe and Gee (2001) marginalized over the variables describing the fractional portions of each pure tissue class and dealt with PV voxels as new set of partial volume classes in segmenting MR images. However, the method does not suit the issue of segmenting infarction lesion from DT-MR images. Low spatial resolution makes it more difficult to discern WM from GM; PV voxels may have the same intensity as pure tissue class. These make the segmentation more difficult in DT-MR images than in conventional MR images. In MSSC, we classified the tissue classes as CSF and background, WM and GM, as well as infarction lesion. Spatial coherence assumptions are included and we have adopted the Markov random field (MRF) as prior model and so the exact computation of the optimal segmentation became intractable. To solve this problem, we detect the tissue edges and reclassify PV voxels after rough statistical classification.

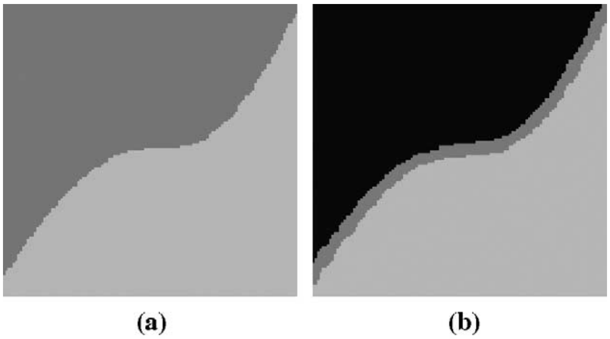

Fig. 4. Possible edges after MSSC. (a) A region comprised of two tissue classes. Some voxels near the edges are misclassified as neighbor class because of PVE. (b) A region comprised of three tissue classes. The strip between two classes shows the misclassified voxels, which have the similar intensity with the third class because of PVE.

As shown in Fig. 4, two possible classification results appear on PV voxels after MSSC. If the intensity of PV voxel is approximate to one pure tissue class, there is a strip between two tissue classes as indicated in b. An additional estimation step is necessary to obtain the fractionation of the pure tissues in each PV voxel.

The tissue boundaries are located in rough-classified DT-MR images by Canny edge detector. It is easy to determine the edge of tissue because of the smooth region of different tissue obtained in previously classified DT-MR images. The edges and their surrounding voxels are treated as possible PV voxels, and we further reclassified the voxels to refine the segmentation.

PV voxels are represented as a linear combination of intensity distributions associated with the K possible tissue classes. The likelihood of the PV voxel can be written as

$$p(y_i|\theta) = \sum_k \pi_{i,k} p_k(y_i|\theta_k) \tag{13}$$

$\theta = \{\theta_i, i\in I\}$, where $\theta_i = (\mu_{k,i}, \sigma_{k,i}), k\in\Lambda\}$, represents the known measurement model parameter set and $\theta = \theta(0)$ is acquired from MSSC. $\pi_{i,k}$ represents the mixing weight of the class k in the mixture at voxel site i.

To determine the fractional amount of specified pure tissue classes within every possible PV voxel, Eq. (13) is solved for $\pi_{i,k}$. Additional constrains are necessary and we make the assumption that each PV voxel stands for a mixture of two tissue types only. For PV voxels consisting of pure classes k_1 and k_2, respectively, Eq. (13) reduces to:

$$p(y_i|\theta) = \pi_{i,k_1} p(y_i|\theta_{k_1}) + \pi_{i,k_2} p(y_i|\theta_{k_2}), \pi_{i,k_1} + \pi_{i,k_2} = 1 \tag{14}$$

$\theta^l_i = (\mu^l_{k,i}, \sigma^l_{k,i})$, $k \in \Lambda$, represents the mean intensity and the standard deviation of class k in the local neighborhood region R^l_i of site i with a diameter r.

$$\mu^l_{k,i} = \frac{\sum_{i \in R^l_i} \mu_{k,i}}{|R^l_{k,i}|}, \sigma^l_{k,i} = \frac{\sum_{i \in R^l_i} \left(y_i - \mu^l_{k,i}\right)^2}{|R^l_{k,i}|} \quad (15)$$

where $|R^l_{k,l}|$ denotes the total number of voxels belonging to tissue class k in region R^l_i. To overcome intensity inhomogeneities, we use θ^l_i instead of θ_i in Eq. (14).

$$p\left(y_i|\theta^l\right) = \pi_{i,k_1} p\left(y_i|\theta^l_{k_1}\right) + \pi_{i,k_2} p\left(y_i|\theta^l_{k_2}\right), \pi_{i,k_1} + \pi_{i,k_2} = 1 \quad (16)$$

As the intensity distribution y and the measurement model parameter set θ for every pure tissue classes are known in prior adaptive statistical classification, we calculate $\theta^l_i = (\mu^l_{k,i}, \sigma^l_{k,i})$, $k \in \Lambda$, using Eq. (15), and the PV voxel at location i, consisting of tissues k_1 and k_2, can be obtained by solving Eq. (16) for $\pi_{i,k}$. At every location i of the edges, k_1 and k_2 are selected according to the two largest numbers of voxels with the same tissue class in the region R^l_i. With known $\pi_{i,k}$, we reclassify possible PV voxel as a certain tissue type.

Pseudocodes

To estimate the tissue classes in DT-MR images, a series of consecutive segmentation at different scale level and partial volume classification is needed. To begin the algorithm, a starting configuration of $x(n)$ is obtained from a rough segmentation that is initially from region splitting and merging at the highest scale level n. Before region splitting and merging, we confirmed the number of classes K and the maximum number of total regions. We split the blurred image into M/16 regions, where M is the total number of voxels in the image; and we merge the regions into K tissue classes. Based on initial rough segmentation, we can get the accurate segmentation from the original image with the highest spatial resolution in scale space by MSSC and PVVR with Eqs. (6), (7), (9), (11), (12), (15) and (16).

The pseudocode for complete segmentation algorithm is as follows:

```
Begin
Set $t = n$, get the blurred patient image at scale level $n$
Initialize segmentation with algorithm of region splitting and merging
Find $\theta(n)$ using initial segmentation
Set $t = n-1$
Set flips = LARGE
While (flips > threshold)
    Get the blurred patient image and FA map at scale level $t$
    flips = 0
    For all sites $i \in I$
        Find $x_i(t)$ based on $U_i(t)$ and $\alpha_i(t)$
        If ( $x_i(t)$ is not previous class $x_i(t+1)$ )
        flips = flips +1
    Repeat for all $i$
    Find $\theta(t)$ using segmentation $x(t)$
    If ($t > 0$) $t = t-1$
End while
Detect the edge of tissues
Calculate $\theta^l_i$
Determine $\pi_{i,k}$
Reclassify the possible PV voxels to get the final segmentation
End
```

Evaluation of MSSC–PVVR method on synthetic data

A 128 × 128 image square was developed and divided into four regions with three tissue classes to test our synthetic image algorithm. The gray value is from 0 to 255. The image was filtered by two or four voxel Gaussian filter in variable radius for constructing it with different PVE; random noise was added upon each test to generate various signal-to-noise (SNR). Here SNR is defined as

$$\text{SNR} = \text{mean interclass contrast/standard deviation of the noise}$$

We compared the performance of our MSSC–PVVR method with threshold segmentation, adaptive maximum a prior (MAP), MSSC on the synthetic images. Adaptive MAP method was described in the Appendix (Rajapakse and Kruggel, 1998; Rajapakse et al., 1997). Mean false-positive rate (FPR), mean true positive rate (TPR), and misclassification ratio (MCR) were calculated for quantitative evaluation of adaptive MAP method and MSSC–PVVR method. MCR is defined as

$$\text{MCR} = \text{number of misclassified voxels/total number of voxels}$$

For the ideal classification, FPR = 0, TPR = 1, and MCR = 0. Because the purpose is to evaluate the effect of MSSC–PVVR method in overcoming PVE and noise disturbance on tissue classification, here we set $\gamma = 0$ in Eq. (11). Receiver operating characteristic (ROC) curves are generated to show the validity of MSSC–PVVR against noise and PVE.

Evaluation of MSSC–PVVR method on real DT-MRI data

The automatic segmentation results were compared with the manual region tracing results to validate MSSC–PVVR method on real DT-MRI data. Several stoke patients with different size and site of infarction were chosen for quantitative evaluation by radiologists. The results were quantified by the similarity index derived from a reliability measurement known as kappa statistic described by Atkins and Mackiewich (1998) and Zijdenbos et al. (1994). Consider a binary segmentation as a set A containing the voxels that are considered to belong to the classification. The similarity of two segmentations A_1 and A_2 is given by a real number $S \in \{0,\ldots,1\}$ that is defined by

$$S = 2\frac{|A_1 \cap A_2|}{|A_1| + |A_2|} \quad (17)$$

Results

Our new unsupervised segmentation method has been applied to both synthetic and real DT-MR images to evaluate the algorithm. For synthetic data, the algorithm comes very close to perfect classification. Moreover, the results from collected data indicate that the algorithm works well on real data. The segmentation algorithm was implemented in the C programming language.

Synthetic data

The performance of the proposed method was compared with others on the simulated data, as shown in Fig. 5. The original image is indicated in Fig. 5a with SNR 5.2. Fig. 5b is the result

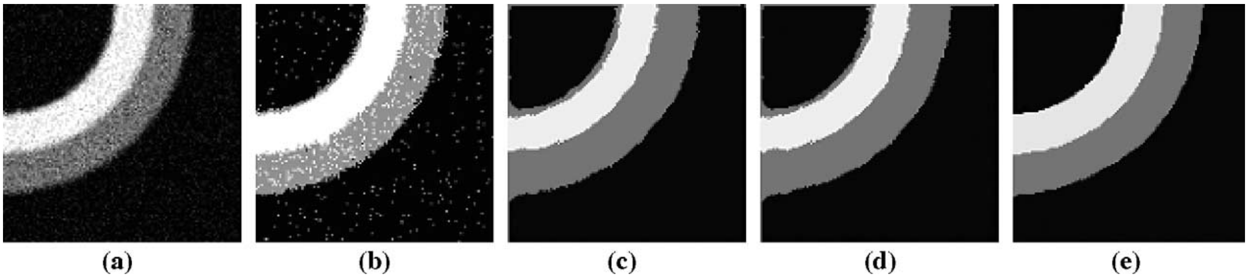

Fig. 5. Comparison of different segmentation methods. (a) Original image with SNR 5.2. (b) Segmentation result by threshold method. (c) Segmentation result by adaptive MAP segmentation. Panel c is initialized by b. (d) Segmentation result by MSSC method. (e) Segmentation result by MSSC–PVVR method.

from threshold segmentation; Fig. 5c adaptive maximum a prior (MAP); Fig. 5d MSSC; and Fig. 5e MSSC–PVVR. To specifically compare the effectivity of overcoming PVE and noise disturbance on tissue classification, we set $\gamma = 0$ in Eq. (11) of MSSC–PVVR method. In Figs. 5c, d, and e, obvious difference can be seen where an incorrect layer of gray tissue has been introduced between the dark background and the light regions due to PVE. The results showed that MSSC–PVVR significantly reduces artifacts introduced by adaptive MAP or MSSC at the boundaries of materials.

On synthetic images with different PVE and SNR, we qualitatively and quantitatively compared the validity of the methods in Table 1. Mean FPR, mean TPR, and MCR were calculated, respectively. It is clear that with more serious PVE, mean FPR and MCR are higher, and mean TPR is lower; misclassification is increased with noise disturbance as well. The accuracy of MSSC–PVVR is significantly higher than adaptive MAP and MSSC in terms of effectively reducing PVE and noise. For example, if the original synthetic image is added by random noise (SNR = 5.2) and filtered by Gaussian filter of four voxels radius, FPR of adaptive Map, MSSC, and MSSC–PVVR are 16.57%, 16.51%, and 10.45%, respectively.

To further clarify the robustness of MSSC–PVVR against noise and PVE, ROC curves of MSSC–PVVR method are depicted as in Fig. 6. Fig. 6a shows the ROC curves corresponding to case 1 (SNR = 28.3), case 2 (SNR = 12.2), and case 3 (SNR = 5.2), respectively. Fig. 6b shows the ROC curves corresponding to case 1 and case 2 with the same SNR = 28.3 and different PVE. With this comparison, we can conclude that the MSSC–PVVR method is robust to noise and PVE.

Real DT-MRI data

The segmentation algorithm has been used to segment DT-MRI scans of 20 patients with clinically diagnosed brain infarction. In acute and subacute stage of stroke, the cerebral infarct signals are hyperintensive in diffusion images. Here we divided the image into three classes $K = 3$, background and CSF, WM and GM, and infraction lesion.

Fig. 7 indicates the segmentation results using the MSSC method at different scale level in the scale space. Columns a and c are the original diffusion tensor images at decreasing levels in scale space. Scale level $t = \{20, 15, 10, 5, 3, 0\}$ is chosen to be displayed, which denotes the number of anisotropic diffusion filtering of the image. The image (a-1) shows the highest scale level $t = 20$; the image (c-3) shows the lowest scale level $t = 0$. It is clear that the increased spatial resolution associated with decreased scale level. Columns b and d indicate the segmentation results at the corresponding levels. Constant Ks = 10 is applied in the anisotropic diffusion filter. Constants $\beta = 0.25$, $\gamma = 0.05$, and $a = 255$ are chosen by experience. Using the segmentation result at scale level $t + 1$ as the initial segmentation, we get the segmentation result at scale level t. When scale level $t = 0$ is reached, the final segmentation is obtained accordingly. In all of our experiments, the highest scale level n is no more than 20.

To compare the proposed method with others on real data, randomly selected DT-MR images from patients with infarction lesion were segmented by different methods: (1) Adaptive MAP; (2) MSSC; (3) MSSC–PVVR. The results are illustrated in Figs. 8–10. The result of adaptive MAP depended on a good initial segmentation. With a bad initialization, the MSSC or MSSC–PVVR method will get much better results than adaptive MAP. With the initialization by region splitting and merging, MSSC and MSSC–PVVR are more robust and convenient. Moreover, adaptive MAP makes misclassification due to the overlapping intensity between infarction lesion and nerve tracts in DT-MR images, while the MSSC method successfully overcomes intensity overlapping by using diffusion anisotropy information from FA map. Using MSSC–PVVR, PV voxels are mostly detected and can be classified more accurately as shown in Figs. 8c, d, 9c, d, and 10c, d. It confirms that PVVR is necessary and effective.

Table 1
Comparative FPR, TPR, and MCR for three algorithms: adaptive MAP, MSSC, and MSSC–PVVR

Case	SNR	Radius of Gaussian filter[a]	Adaptive MAP			MSSC			MSSC–PVVR		
			FPR (%)	TPR (%)	MCR (%)	FPR (%)	TPR (%)	MCR (%)	FPR (%)	TPR (%)	MCR (%)
1	28.3	2	8.87	96.39	4.55	8.83	96.85	4.53	7.74	97.59	3.24
2	12.2	2	9.97	96.31	4.63	9.94	96.42	4.61	7.94	97.43	3.43
3	5.2	2	10.23	96.10	4.74	10.11	96.11	4.71	8.21	97.08	3.68
4	28.3	4	15.39	94.24	7.89	15.36	94.24	7.80	10.28	95.95	4.66
5	12.2	4	15.86	94.08	8.05	15.82	94.11	8.01	10.32	95.73	4.73
6	5.2	4	16.57	93.87	8.36	16.51	94.00	8.25	10.45	95.56	4.87

[a] The image was filtered by Gaussian filter in variable radius for different PVE.

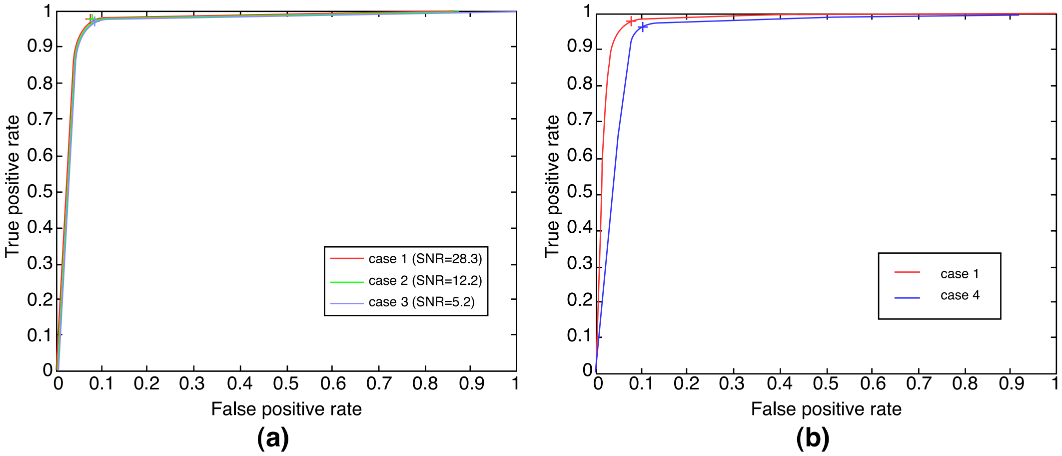

Fig. 6. ROC curves of MSSC–PVVR method. (a) ROC curves for cases 1, 2, and 3 with various SNR and the same PVE. (b) ROC curves for cases 1 and 4 with the same SNR and different PVE.

Now Zijdenbos et al. (1994) state that although $S > 0.7$ indicates excellent agreement, it is difficult to interpret the absolute value of S (Atkins and Mackiewich, 1998). Fig. 11 illustrates the comparison of manual segmentation and automatic MSSC–PVVR segmentation method. Table 2 lists both manually and automatically segmented infarction lesion voxels, and similarity index as well. The similarity between MSSC–PVVR and the expert's manual outlined lesion region was very high—always above 0.92, best at 0.98. Two independent manual segmentations were performed by radiologists to measure the intra-observer accuracy, and the similarity is around 0.97.

Discussions

In MSSC–PVVR, the Gaussian assumption for random noise is applied (Laidlaw et al., 1998; Marroquin et al., 2002; Martel et al., 1999; Noe and Gee, 2001; Rajapakse and Kruggel, 1998; Shattuch

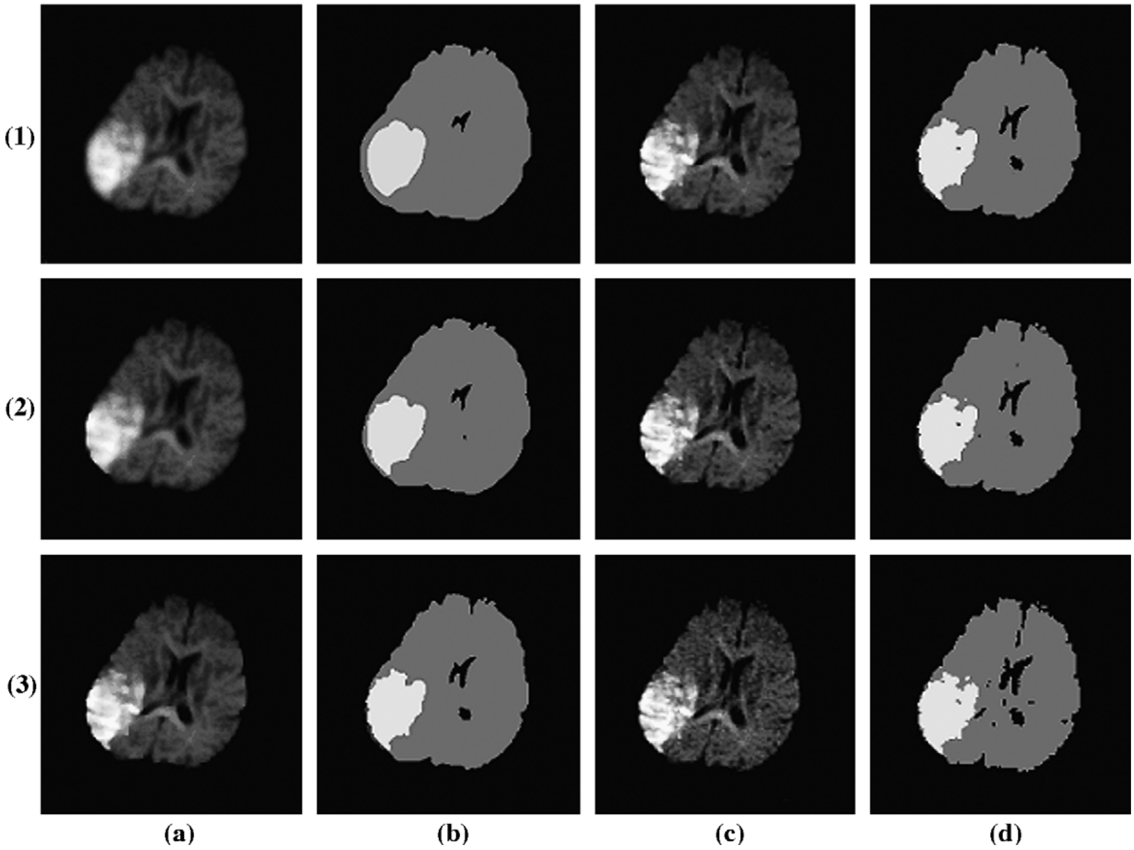

Fig. 7. Segmentation obtained by MSSC method at different scale levels. Columns a and c show the diffusion images at a decreasing scale level. Scale level $t = \{20, 15, 10, 5, 3, 0\}$ is chosen to displayed here. The image (a-1) shows the highest scale level $t = 20$; the image (c-3) shows the lowest scale level $t = 0$. Columns b and d are the segmentation results at the corresponding scale levels.

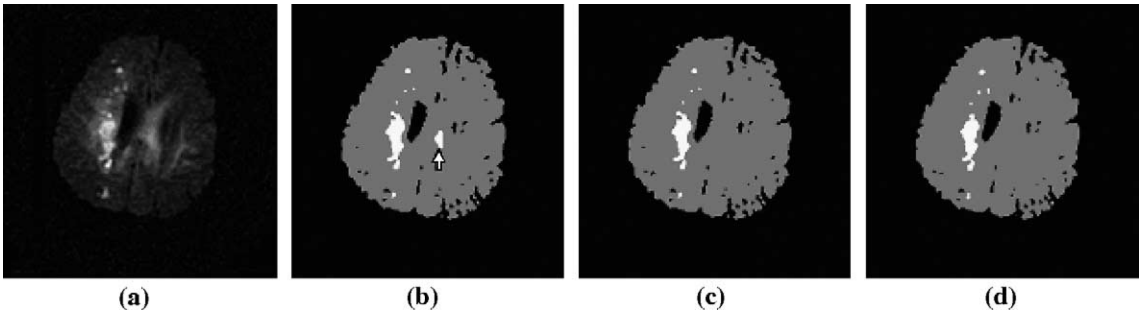

Fig. 8. Segmentation obtained by different methods. (a) Original cerebral DT-MR image of infarction lesion acquired with 3.0 T. (b) Segmentation by adaptive MAP. The block arrow points to misclassified nerve tract. (c) Segmentation by MSSC. (d) Segmentation by MSSC–PVVR.

et al., 2001). Segmentation results were obtained from MSSC by using both the measurement model and a prior model at different scale level. A MRF is applied as prior model to impose the continuity and homogeneity constraints of tissue regions, which is similar as Rajapakse and Kruggel (1998), so the false positive in lesion classification is successfully reduced. Incorporation of the discontinuity process into the prior model may improve segmentation result, but the calculation is more complicated. Using tissue-specific and spatial-dependent means and standard deviations as parameters in the measurement model (Rajapakse and Kruggel, 1998), biological variations and spatial intensity variations are accounted for.

The ICM algorithm adopted by Rajapakse et al. (1997) and Martel et al. (1999) converges on a local minimum of the energy function in a few iterations. The initial segmentation is important for ICM. If the initial configuration is far from the optimal configuration, the final segmentation may end in a local minimum. Manual segmentation has been employed sometimes to get an acceptable initialization even it is labor intensive. We advanced ICM algorithm by scale space. From coarse level to fine level in scale space, we get the accurate segmentation in infarction lesion step by step and the susceptibility artifacts are mostly removed at the same time. The MSSC method is an iterative process. We iteratively get the model parameters of the image at lower spatial resolution and use these parameters to determine the tissue class of next image at higher resolution until final segmentation of original image is obtained. MSSC or MSSC–PVVR is less influenced by the initial segmentation. Rough region splitting and merging are sufficient to initialize MSSC or MSSC–PVVR. Moreover, by incorporating the information from the FA map, the MSSC model can adaptively adjust the energy value according to diffusion anisotropy, so the misclassification caused by diffusion anisotropy in DT-MR images can be avoided.

Partial volume voxel reclassification is applied after MSSC to overcome PVE accounting for RF inhomogeneities. PVE exists at the tissue boundaries of the DT-MR images. A complication in PVE is that the combined voxels of infarction lesions and CSF or background may result in similar intensities to WM or GM. The PVVR model was proposed to overcome PVE that presents at the tissue boundaries of the image. To account for RF inhomogeneities, PV voxels are reclassified based upon means and standard deviations of local region other than of whole tissues, that is, different from other researchers (Laidlaw et al., 1998; Noe and Gee, 2001; Shattuch et al., 2001). MSSC–PVVR is more accurate than adaptive MAP and MSSC because PVE is greatly diminished by PVVR.

The segmentation results by threshold, adaptive MAP, MSSC, and MSSC–PVVR are analyzed on both synthetic data and real DT-MRI data, respectively. On synthetic images with different PVE and SNR, the validity of each method has been compared both qualitatively and quantitatively. From Table 1, it is clear that if the PVE is more serious, the mean FPR and MCR will be higher, and the mean TPR will be lower. Moreover, misclassification is increased with noise disturbance. The accuracy of MSSC–PVVR is significantly higher than adaptive MAP and MSSC in terms of effectively reducing PVE and noise. For example, if the original synthetic image is added by random noise and filtered with Gaussian filter of four voxels radius, FPR of adaptive Map, MSSC, and MSSC–PVVR is 16.57%, 16.51%, and 10.45%, respectively. As shown in Figs. 8–10, the segmentation results confirmed that MSSC–PVVR can overcome intensity overlapping in infarct lesion and nerve tract; is less sensitivity to initialization, noise, and RF inhomogeneities; and can well overcome PVE. Analysis of DT-MRI scans in 20 patients with clinically diagnosed infarction was carried out. The automated method results in a satisfied segmentation of infarction lesion even with the presence of noise and RF inhomogeneities of scanners. The

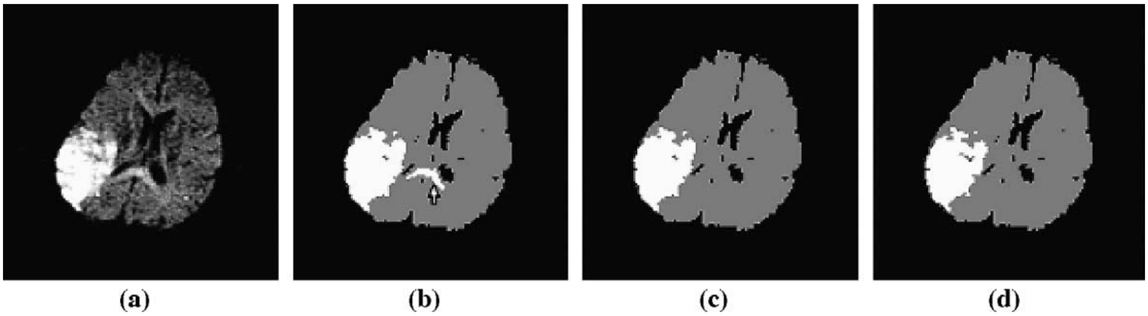

Fig. 9. Segmentation obtained by different methods. (a) Original cerebral DT-MR image of infarction lesion acquired with 1.5 T. (b) Segmentation by adaptive MAP. The block arrow points to misclassified nerve tract. (c) Segmentation by MSSC. (d) Segmentation by MSSC–PVVR.

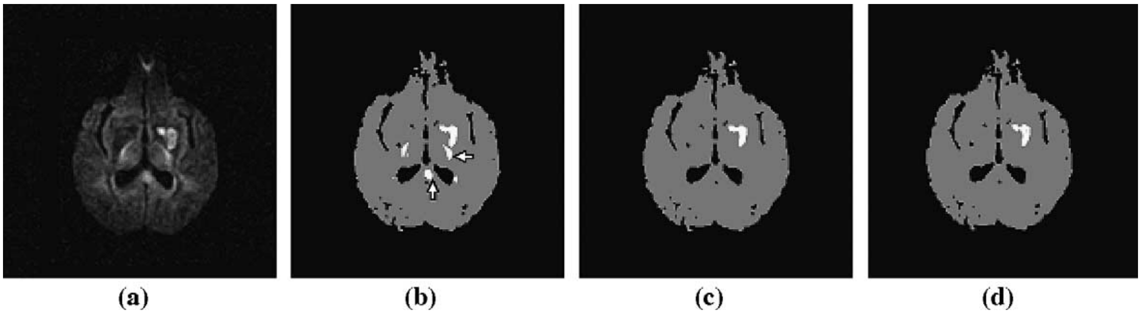

Fig. 10. Segmentation obtained by different methods. (a) Original cerebral DT-MR image of infarction lesion acquired with 3.0 T. (b) Segmentation by adaptive MAP. The block arrow points to misclassified nerve tract. (c) Segmentation by MSSC. (d) Segmentation by MSSC–PVVR.

automated method was quantitatively compared with lesion delineations by clinical experts. In Table 2, the similarity index between automatic and manual segmentation is high, always above 0.92. The automatic MSSC–PVVR method highly matches the manual segmentation, which confirms its accuracy and reproducibility in terms of identifying infarction lesion.

DT-MRI study in both experiments and real stroke patient suggests that DT-MRI may provide useful information for disease evolution (Sotak, 2002) by calculating mean apparent diffusion coefficient (ADC), FA, and lattice index (LI) in normal and stroke lesion regions. This quantitative information is valuable in distinguishing old and new lesions (Gonzalez et al., 1999; Martel et al., 1999; Sotak, 2002) and in assisting accurate diagnosis and prognosis in stroke (Lie et al., 2004; O'Sullivan et al., 2004; Sotak, 2002). Unsupervised segmentation method of MSSC–PVVR makes the procedure feasible, convenient, and reproducible. It may play an important role in the clinical evaluation of stroke treatments.

Conclusions

In summary, we have presented a novel MSSC–PVVR framework of automatically segmenting brain infarction lesion from DT-MR images. The method can overcome the problem of intensity overlapping caused by diffusion anisotropy, and it was proven robust even in the presence of noise, PVE, and RF inhomogeneities. We validated the MSSC–PVVR method on both synthetic images and real DT-MR images. Moreover, the accuracy and reproducibility have been confirmed by clinical experts. The application of DT-MRI combined with our unsupervised segmentation method may play an important role in the clinical evaluation of new stroke treatments.

Acknowledgments

This paper is supported by the National Science Fund for Distinguished Young Scholars of China under Grant No. 60225008, the Special Project of National Grand Fundamental Research 973 Program of China under Grant No. 2002CCA03900, the National Natural Science Foundation of China under Grant Nos. 90209008, 60172057, 30370418, 30270403, 60302016, and the National High Technology Development Program of China under Grant No. 2002AA234051.

Appendix A

Rajapakse et al. (1997) introduced the segmentation method of adaptive MAP estimation in details as described below. The process of segmentation is to find x that represents the correct tissue class at each voxel site given by image y. We attempt to find the MAP estimation from the image data. Here $p(x|y)$ is the posterior density of the segmentation x given the image y. Because the prior probability of image $p(y)$ is independent of the segmentation x, from Bayesian theorem

$$p(x|y) \propto p(x,y) = p(y|x)p(x) \tag{19}$$

The image data at a particular site i represents a noise-corrupted version of the signature of the tissue class at that voxel.

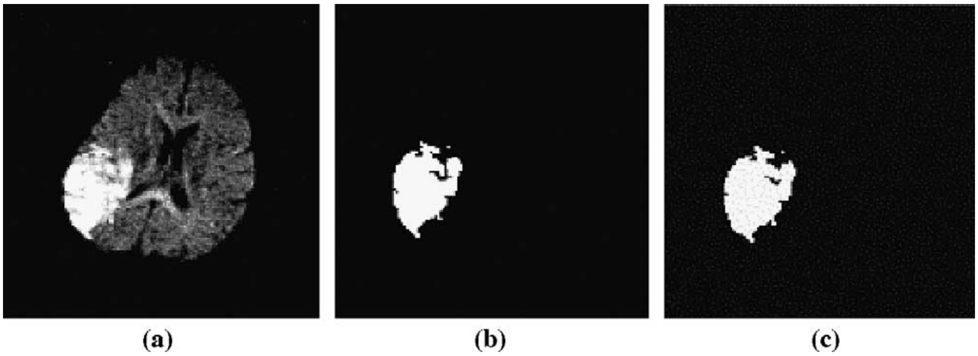

Fig. 11. Comparison of manual segmentation and automatic MSSC–PVVR segmentation in infarction lesion. (a) Original diffusion MR image. (b) Manual segmentation by radiologist. (c) Automatic segmentation by MSSC–PVVR method. The similarity index of b and c is 0.973.

Table 2
Comparison of manual and automatic segmentation of infarction lesion

Patient	Slice number	Manual area (voxel)	Auto area (voxel)	Similarity index
1	11	619	654	0.973
	13	437	471	0.952
2	11	115	128	0.944
	12	44	50	0.931
3	12	954	994	0.978
	14	782	817	0.963

We assume that the noise is additive, white, Gaussian, tissue dependent, and space variant. Here $\mu_{k,i}$, $n_{k,I}$, and $\sigma_{k},_{i}$, respectively, represent the mean image intensity of class k at site i, the noise signal at site i for tissue class k, and the standard deviation of the noise for the tissue class k at site i. The measurement model is characterized by the parameter set $\theta = \{\theta_i, i \in I\}$, where $\theta_i = \{\theta_{k,i} = (\mu_{k,i}, \sigma_{k,i}), k \in \Lambda\}$.

If R_k denotes the region or the set of all voxel sites belonging to tissue class k, then the conditional density $p(y|x)$ can be written as

$$p(y|x) = \prod_k \prod_{i \in R_k} p_k(y_i|\theta_{k,i}) = \prod_k \prod_{i \in R_k} \frac{1}{\sqrt{(2\pi)}\sigma_{k,i}} \exp\left\{ -\frac{1}{2}\left(\frac{y_i - \mu_{k,i}}{\sigma_{k,i}}\right)^2 \right\} \tag{20}$$

The probability density of x is given by a Gibbs distribution (German and Geman, 1984; Pappas, 1992), having the form

$$p(x) = \exp\left\{ -\beta \sum_{c \in C} V_c(x) \right\} \tag{21}$$

where β is a normalizing constant and the summation is taken over all the cliques C over the image. A clique is a set of points that are neighbors of one another.

By substituting Eqs. (20) and (21) in Eq. (19) and omitting the constant factors, the posterior probability is

$$p(x|y) \propto \exp\{-U(x)\} \tag{22}$$

where the energy function $U(x)$

$$U(x) = \frac{1}{2} \sum_k \sum_{i \in R_k} \left(\frac{y_i - \mu_{k,i}}{\sigma_{k,i}}\right)^2 + \sum_k \sum_{i \in R_k} \log(\sigma_{k,i}) + \beta \sum_{c \in C} V_c(x) \tag{23}$$

The problem of finding the MAP estimate of the segmentation is same as the minimization problem of the energy function $U(x)$.

References

Atkins, M.S., Mackiewich, B., 1998. Fully automatic segmentation of the brain in MRI. IEEE Trans. Med. Imag. 17 (1), 98–107.

Baird, A.E., Benfield, A., Schlaug, G., Siewert, B., Lovblad, K.O., Edelman, R.R., Warach, S., 1997. Enlargement of human cerebral ischemic lesion volumes measured by diffusion-weighted magnetic resonance imaging [see comments]. Ann. Neurol. 41, 581–589.

Barber, P.A., Darby, D.G., Desmond, P.M., Yang, Q., Gerraty, R.P., Jolley, D., Donnan, G.A., Tress, B.M., Davis, S.M., 1998. Prediction of stroke outcome with echoplanar perfusion- and diffusion-weighted MRI. Neurology 51, 418–426.

Canny, J., 1986. A computational approach to edge detection. IEEE Trans. Pattern Anal. Mach. Intell. 8, 679–698.

Escoda, O.D., Petrovic, A., Vandergheynst, P., 2002. Segmentation of natural images using scale-space representations: a linear and a nonlinear approach. Proc. of EUSIPCO 2002.

German, S., Geman, D., 1984. Stochastic relaxation, Gibbs distribution, and the Bayesian restoration of images. IEEE Trans. Pattern Anal. Mach. Intell. 6, 721–741.

Gonzalez, R.G., Schaefer, P.W., Buonanno, F.S., Schwamm, L.H., Budzik, R.F., Rordorf, G., Wang, B., Sorensen, A.G., Koroshetz, W.J., 1999. Diffusion-weighted MR imaging: diagnostic accuracy in patients imaged within 6 hours of stroke symptom onset. Radiology 210, 155–162.

Laidlaw, D.H., Fleischer, K.W., Barr, A.H., 1998. Partial-volume Bayesian classification of material mixtures in MR volume data using voxel histograms. IEEE Trans. Med. Imag. 17 (1), 74–87.

Le Bihan, D., Mangin, J.F., 2001. Diffusion tensor imaging: concepts and application. J. Magn. Reson. Imaging 13, 534–546.

Leemput, K.V., Maes, F., Vandermeulen, D., Suetens, P., 1999a. Automated model-based tissue classification of MR images of the brain. IEEE Trans. Med. Imag. 18 (10), 897–908.

Leemput, K.V., Maes, F., Vandermeulen, D., Suetens, P., 1999b. Automated model-based bias field correction of MR images of the brain. IEEE Trans. Med. Imag. 18 (10), 885–896.

Leemput, K.V., Maes, F., Vandermeulen, D., Colchester, A., Suetens, P., 2001. Automated segmentation of multiple sclerosis lesions by model outlier detection. IEEE Trans. Med. Imag. 20 (8), 677–688.

Lie, C., Hirsch, J.G., Rossmanith, C., 2004. Clinicotopographical correlation of corticospinal tract stroke: a color-coded diffusion tensor imaging study. Stroke (United States) 35 (1), 86–92.

Lovblad, K.O., Baird, A.E., Schlaug, G., Benfield, A., Siewert, B., Voetsch, B., Connor, A., Burzynski, C., Delman, R.R., Warach, S., 1997. Ischemic lesion volumes in acute stroke by diffusion-weighted magnetic resonance imaging correlate with clinical outcome. Ann. Neurol. 42, 164–170.

Lovblad, K.O., Laubach, H.J., Baird, A.E., Curtin, F., Schlaug, G., Edelman, R.R., Warach, S., 1998. Clinical experience with diffusion-weighted MR in patients with acute stroke [see comments]. AJNR Am. J. Neuroradiol. 19, 1061–1066.

Marroquin, J.L., Vemuri, B.C., Botello, S., Calderon, F., Fernandez-Bouzas, A., 2002. An accurate and efficient Bayesian method for automatic segmentation of brain MRI. IEEE Trans. Med. Imag. 21 (8), 934–945.

Martel, A.L., Allder, S.J., Delay, G.S., Morgan, P.S., Moody, A.R., 1999. Measurement of infarct volume in stroke patients using adaptive segmentation of diffusion weighted MR images. MICCAI′ 99 1679, 22–31.

Moon, N., Bullitt, E., Leemput, K.V., Gerig, G., 2002. Automatic brain and tumor segmentation. MICCAI2002 2488, 372–379.

Mukherjee, P., Bahn, M.M., Mckinstry, R.C., 2000. Differences between gray matter and white matter water diffusion in stroke: diffusion-tensor MR imaging in 12 patients. Radiology 215, 211–220.

Noe, A., Gee, J.C., 2001. Partial volume segmentation of cerebral MRI scans with mixture model clustering. IPMI2001, 423–430.

O'Sullivan, M., Morris, R.G., Huckstep, B., 2004. Diffusion tensor MRI correlates with executive dysfunction in patients with ischaemic leukoaraiosis. J. Neurol., Neurosurg. Psychiatry (England) 75 (3), 441–447.

Pappas, T.N., 1992. An adaptive clustering algorithm for image segmentation. IEEE Trans. Signal Process. 40 (4), 901–914.

Perona, P., Malik, J., 1990. Scale-space and edge detections using anisotropic diffusion. IEEE Trans. Pattern Anal. Mach. Intell. 12 (7), 629–639.

Rajapakse, J.C., Kruggel, F., 1998. Segmentation of MR images with intensity inhomogeneities. Image Vis. Comput. 16 (3), 165–180.

Rajapakse, J.C., Giedd, J.N., Rapoport, J.L., 1997. Statistical approach to segmentation of single-channel cerebral MR images. IEEE Trans. Med. Imag. 16 (2), 176–186.

Schnabel, J.A., Arridge, S.R., 1996. Multi-scale shape description of MR brain images using active contour models. Proc. SPIE Med. Imag. 2710, 596–606.

Shattuch, D.W., Sandor-Leahy, S.R., Schaper, K.A., Rottenberg, D.A., Leahy, R.M., 2001. Magnetic resonance image tissue classification using a partial volume model. NeuroImage 13, 856–876.

Sorensen, A.G., Wu, O., Copen, W.A., 1999. Human acute cerebral ischemia: detection of changes in water diffusion anisotropy by using MR imaging. Radiology 212, 785–792.

Sotak, C.H., 2002. The role of diffusion tensor imaging in the evaluation of ischemic brain injury—A review. NMR Biomed. (England) 15, 561–569.

Warfield, S.K., Robatino, A., Dengler, J., Jolesz, F.A., Kikinis, R., 1999. Nonlinear registration and template driven segmentation. Brain Warping. Academic Press, San Diego, pp. 67–84. Ch. 4.

Warfield, S.K., Kaus, M., Jolesz, F.A., Kikinis, R., 2000. Adaptive, template moderated, spatially varying statistical classification. Med. Image Anal. 4 (1), 43–55.

Westin, C.F., Maier, S.E., Mamata, H., 2002. Processing and visualization for diffusion tensor MRI. Med. Image Anal. 6, 93–108.

Wiegell, M.R., 2003. Automatic segmentation of thalamic nuclei from diffusion tensor magnetic resonance imaging. NeuroImage 19, 391–401.

Zijdenbos, A.P., Dawant, B.M., Margolin, R.A., Palmer, A.C., 1994. Morphometric analysis of white matter lesions in MR images: method and validation. IEEE Trans. Med. Imag. 13, 716–724.